Sedimentary Geology 217 (2009) 128–139

Contents lists available at ScienceDirect

Sedimentary Geology

journal homepage: www.elsevier.com/locate/sedgeo

Manganese nodules in the Miocene Bahía Inglesa Formation, north-central Chile: Petrography, geochemistry, genesis and palaeoceanographic significance

L.E. Achurra [a,b], J.P. Lacassie [b,c], J.P. Le Roux [a,*], C. Marquardt [b,d], M. Belmar [a,e], J. Ruiz-del-Solar [f], S.E. Ishman [g]

[a] Departamento de Geología, Facultad de Ciencias Físicas y Matemáticas, Universidad de Chile, Casilla 13518, Correo 21, Santiago, Chile
[b] SERNAGEOMIN, Av. Santa Maria 0104, Providencia, Santiago, Chile
[c] Palaeoproterozoic Mineralization Research Group, Department of Geology, University of Johannesburg, Auckland Park, Johannesburg, 2006, South Africa
[d] Antofagasta Minerals, Paseo Ahumada 11, Oficina 602, Santiago, Chile
[e] SGS Mineral Services, Puerto Madero 9600, Pudahuel, Santiago, Chile
[f] Departamento de Ingeniería Eléctrica, Facultad de Ciencias Físicas y Matemáticas, Universidad de Chile, Casilla 412-3, Santiago, Chile
[g] Department of Geology, Southern Illinois University, Carbondale, IL 62901-4324, USA

ARTICLE INFO

Article history:
Received 10 September 2008
Received in revised form 25 March 2009
Accepted 27 March 2009

Keywords:
Manganese nodules
Bahía Inglesa Formation
Upwelling
Multiple discriminant analysis
Neuron network analysis

ABSTRACT

Manganese nodules recovered from two stratigraphic horizons of Tortonian–Messinian (late Miocene) age in the Bahía Inglesa Formation of north-central Chile were studied using XRD, SEM and geochemical analysis. The dominant mineral in the nodules is todorokite, which suggests a diagenetic, marine environment. This is supported by field observations of nodules replacing *Ophiomorpha* burrows. Preliminary, traditional statistical analysis of the nodule geochemistry, including single element, binary and ternary ratios, suggests that the nodules are of the supergene, deep marine type, as also indicated by the presence of foraminifers typical of the upper continental slope, as well as debris flow and turbidity current deposits in an associated submarine palaeocanyon. However, abnormally low Cu concentrations seem to contradict this interpretation, so that additional analyses were carried out. This included multiple discriminant analysis (MDA), as well as a new technique applied for the first time to manganese nodules, namely artificial neural network analysis (ANN). In both methods central log-ratio (CLR) normalization was applied to the raw data. The results, in particular those of the ANN analysis, suggest that the Bahia Inglesa nodules present a chemical signature distinct from that of nodules described to date. A new class is therefore proposed, namely supergene intermediate marine (partially restricted basin).

1. Introduction

Manganese nodules were first discovered in 1873 during a cruise of the HMS Challenger. Since then, they have been found associated with micro-concretions, coatings and crusts, at almost all depths and latitudes in all the oceans of the world, as well as in some lakes (Crerar and Barnes, 1974; Giresse et al., 1998; Banerjee et al., 1999; Banerjee and Miura, 2001; Hlawatsch et al., 2002). The nodules are especially common in the Pacific Ocean (Jung and Lee, 1999; Hu et al., 2002; Bu et al., 2003), where it is estimated that they cover approximately 10–30% of the deep ocean floor (Menard and Shipek, 1958). Their distribution generally coincides with temperate waters north and south of the equator, where adjacent lands release plentiful amounts of manganese and iron through their river systems (Cronan, 1977; Duff, 1993).

Oceanic manganese nodules are normally confined to the sediment surface or just below it and range in diameter from less than 1 mm to 5 cm (Morales, 1984; Duff, 1993), but coalescing concretionary slabs and very large nodules up to 1 m in diameter have been found. Their rate of growth varies from about 1 to 200 mm/my (Roy, 1992), being normally in the range of 3–4 mm/my (Duff, 1993). Cross-sections commonly display crude growth rings representing temporal textural and compositional changes.

Because of their slow growth rate, the potential of manganese nodules as indicators of oceanographic variations in the geological past is enormous, although relatively few studies have been carried out in this regard. Hlawatsch et al. (2002) investigated ferromanganese nodules in the western Baltic Sea and detected enhanced heavy metal concentrations (especially Zn) since the end of the 19th century, probably as a result of anthropogenic input. Banakar et al. (1993) studied a nodule from the Somali Basin and recorded important palaeoceanographic events, such as increased Antarctic bottom water flow and an elevated CCD at around 13 Ma, followed by a lowering of the CCD during the late Miocene and an increased influx of eolian dust. At the Miocene/Pliocene boundary, a drastic fall in eolian dust influx was recorded.

The potential of manganese nodules to serve as palaeoenvironmental indicators in ancient sedimentary deposits has not been fully

* Corresponding author. Tel.: +56 2 9784123.
E-mail address: jroux@ing.uchile.cl (J.P. Le Roux).

0037-0738/$ – see front matter © 2009 Elsevier B.V. All rights reserved.
doi:10.1016/j.sedgeo.2009.03.016

Table 1
Classification of manganese nodules.

S: supergene	S_T: supergene terrestrial	S_M: supergene marine	
	S_{TS}: soils and bogs	S_{ME}: epeiric seas (restricted basins)	
	S_{TF}: freshwater lakes and streams	S_{MS}: shallow marine (continental shelf and coastal zone)	
		S_{MD}: deep marine (continental slope, ocean floor and seamounts)	S_{MDS}: siliceous, pelagic ooze (type S of Dymond et al., 1984)
			S_{MDR}: red, pelagic clay (type R of Dymond et al., 1984)
			S_{MDC}: calcareous, pelagic ooze
			S_{MDH}: hemipelagic clay (type H of Dymond et al., 1984)
H: hydrothermal	H_T: hydrothermal terrestrial (hot springs and pools)	H_M: hydrothermal marine (volcanic spreading centers)	

realized. One reason may be that nodules have been reported from only a limited number of pre-Holocene deposits, such as the Miocene in Somali (Banakar et al., 1993), the Cretaceous in Timor (Audley-Charles, 1965), and the Late Palaeoproterozoic in South Africa, where they have been described as Mn-rich oncoids (Schaefer et al., 2001). Another reason may be that the methods applied to date often give ambiguous results. Here we describe the characteristics of manganese nodules in the Miocene Bahía Inglesa Formation of north-central Chile. The mineralogy and geochemistry of the nodules were studied by X-ray diffraction and microprobe analysis. Traditional binary and ternary plots, multiple discriminant analysis (MDA), and a relatively new technique applied for the first time to manganese nodules, artificial neural networks (ANN), were compared to determine which of these methods best reflect the origin and palaeoenvironment of the Bahía Inglesa nodules.

2. Origin, classification and chemical characteristics of manganese nodules

The classification of manganese nodules is based mainly on their genesis or the substrate sediments in which they occur (Dymond et al., 1984; Halbach et al., 1977; 1981; Nicholson, 1992b; Roy, 1992). Table 1 presents a synthesis of existing classification schemes, the four main groups being supergene terrestrial (S_T) and marine (S_M) nodules, and hydrothermal terrestrial (H_T) and marine (H_M) nodules.

Within the supergene marine or S_M group, many researchers also distinguish between hydrogenetic nodules, in which the minerals are supplied directly from the marine water close to the ocean floor, and diagenetic nodules, which form during early diagenesis within a few cm to dm below the sediment/water interface, metals being derived from the interstitial pore water. Both hydrogenetic and diagenetic processes may operate in the same nodule, however (Halbach et al., 1981; Roy, 1992). In such partially buried nodules the growth rate of the bottom, which is subjected to diagenetic processes, may be much higher than that of its hydrogenetic top (Duff, 1993). These nodules commonly have rough bottoms and smooth tops with an equatorial girdle (Raab, 1972; Halbach et al., 1981).

Diagenetic nodules may be either oxic or suboxic, depending on the oxidized or reduced nature of the host sediments (Roy, 1992). Oxic nodules are mainly S_{MDS}, S_{MDR}, or S_{MDC} types, whereas suboxic nodules generally belong to the S_{MDH} class (Table 1).

The physical, mineralogical and chemical characteristics of manganese nodules seem to vary in accordance with the dominating processes and environments in which they occur (Table 2). With regard to shape and surface texture, hydrogenetic nodules are generally polynucleated and irregular (but may also be ellipsoidal or discoidal) with smooth to finely porous surface textures. The dominant manganese mineral is vernadite (δ-MnO_2). These nodules occur preferentially on seamounts (Jung and Lee, 1999; Banerjee and Miura, 2001; Bu et al., 2003), as for example in the Pacific Ocean where their size ranges from 0.5 to 8 cm (Halbach et al., 1981). Diagenetic nodules are commonly ellipsoidal to discoidal with porous-rough to gritty surfaces, todorokite being the dominant mineral. They occur mostly in the deeper parts of basins on siliceous oozes or clays (S_{MDS}), where their sizes range between 1 and 5 cm (Halbach et al., 1981; Marchig et al., 2001). Nodules of mixed diagenetic–hydrogenetic origin, also occurring within the deeper basins of the Pacific Ocean, reach up to 14 cm in diameter and have ellipsoidal to discoidal shapes with botryoidal bottoms and smooth tops (Halbach et al., 1981). In the Central Indian Basin, Banerjee and Miura (2001) reported that small hydrogenetic nodules (<4 cm) with smooth surfaces are more common on red clay, terrigenous and terrigenous-siliceous ooze transition sediments, whereas large diagenetic nodules (>4 cm) with rough surfaces are more prevalent on siliceous ooze, siliceous ooze-red clay, and calcareous ooze-red clay transition zones.

The chemistry of manganese nodules also varies widely according to their origin and sedimentary environment (Table 2). As a consequence, single elements such as Zn and Cu, as well as binary and ternary diagrams, including Mn/Fe, Mg/Na, Co/(Ni + Cu), Fe/(Ni + Cu), and 10(Cu + Ni + Zn), have often been used to characterize the different nodules (e.g., Bonatti et al., 1972; Rona, 1978; Dymond et al., 1984; Roy, 1992; Nicholson, 1992b; Winter et al., 1997; Jung and Lee, 1999; Banerjee et al., 1999). However, the validity of such diagrams has been criticized on the grounds that they assume the data are drawn from a continuous sample space, whereas geochemical data are obtained from a closed sample space in which all variables sum to a constant, usually 100%. This is known as the constant- or closed-sum problem, which can cause errors in the

Table 2
Main characteristics of manganese nodules.

	Hydrogenetic	Diagenetic oxic	Diagenetic suboxic
Dominant occurrence	Seamounts, S_{MDR}, S_{MDS}	Deep-sea basins, S_{MDS}, S_{MDR}, S_{MDC}	Continental slope, S_{MDH}
Shape and texture	Polynucleated, irregular, smooth surface texture, small	Mononucleated, rough surface texture, botryoidal, discoidal, large	Mononucleated, rough surface texture, ellipsoidal, medium
Chemical signature			
Mn/Fe	1.17	7.11	97.96
Co/(Ni + Cu)	0.217	0.017	0.006
Zn/(Ni + Cu)	0.125	0.153	0.396
Dominant mineral	Vernadite	Todorokite	Todorokite
Growth rate	<5 mm/my	16 mm/my	100–200 mm/my

correlation analysis of compositional data (Chayes, 1960; Butler, 1979; Aitchison, 1986; Armstrong-Altrin et al., 2005; Barbera et al., 2009). Nevertheless, it appears that S_{MD} nodules generally have average Fe/Mn ratios higher than those of S_{TF} and S_{ME} nodules, lower than those of S_{MS} nodules, and in-between the high and low ranges of H_M nodules.

3. Geology of the Bahía Inglesa deposits

The Bahía Inglesa Formation crops out along the coast of the Atacama region between about 26°45′ S and 28°S (Fig. 1), where it unconformably overlies Lower Jurassic granitoids and alluvial conglomerates of the Angostura Formation and is in turn overlain unconformably by littoral Holocene deposits known as the Caldera beds. Towards the southeast, it interfingers with fluvial conglomerates and gravels of the Copiapó River (Godoy et al., 2003). The formation is composed mainly of mudrocks, sandstones and coquinas, with some diatomites, phosphorites, conglomerates and breccias, interpreted by Marquardt et al. (2000) as continental shelf deposits and by Achurra (2004) as continental shelf to slope deposits. Of particular importance is the presence of a submarine palaeocanyon with debris flow and turbidity current deposits occurring stratigraphically just below the nodule-bearing beds (Achurra, 2004).

One of the most complete exposures of the Bahía Inglesa Formation occurs in the vicinity of Playa Chorrillos south of the Copiapó Promontory (Fig. 1). At this locality, manganese nodules occur as two distinct units within an interval of about 22 m, consisting mainly of light brown to greenish yellow shale criss-crossed by gypsum veins in the upper part. Fig. 2 shows a measured stratigraphic column at Playa Chorrillos, indicating the stratigraphic position of the unit hosting the nodules.

Below the first nodules is a 270 cm thick, green (yellow-weathering), silty mudstone showing soft-sediment folds in its basal 30 cm. These folds are well oriented, striking between 185° and 225°, and probably resulted from slumping down a west-sloping incline. Some bioturbation in the form of horizontal to oblique tubes is present. The basal nodules occur in a 50 cm thick, light brown, silty mudstone, where their diameter varies from a few mm to more than 3 cm. In shape they are discoidal to almost perfectly spherical, although generally slightly flattened parallel to the bedding. The smaller nodules have smooth surfaces, whereas larger nodules are generally botryoidal in shape (Fig. 3a). Some nodules occur on top of trace fossils (including *Ophiomorpha*), or in rare cases replace the latter completely (Fig. 3b), clearly indicating a diagenetic origin.

The basal nodule unit is overlain by deposits apparently devoid of nodules. These include a 10 cm thick, harder siltstone, followed by a 20-cm thick, light greenish yellow shale, which grades upward into 120 cm of yellowish buff shale, a lenticular, up to 60-cm thick small-pebble conglomerate and finally 160 cm of buff-colored, poorly exposed shale.

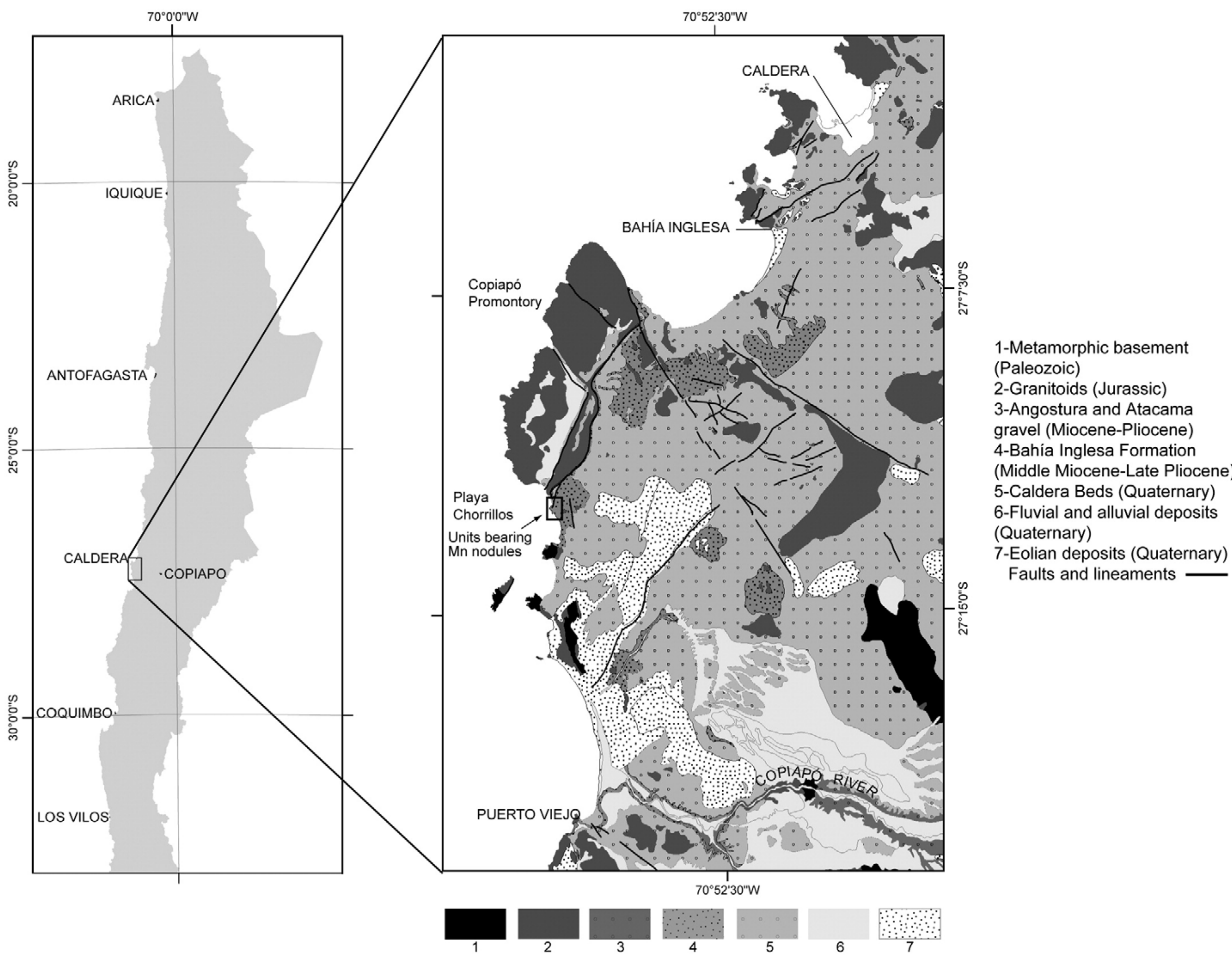

Fig. 1. Geology of the coastal Atacama region between Caldera and Puerto Viejo.

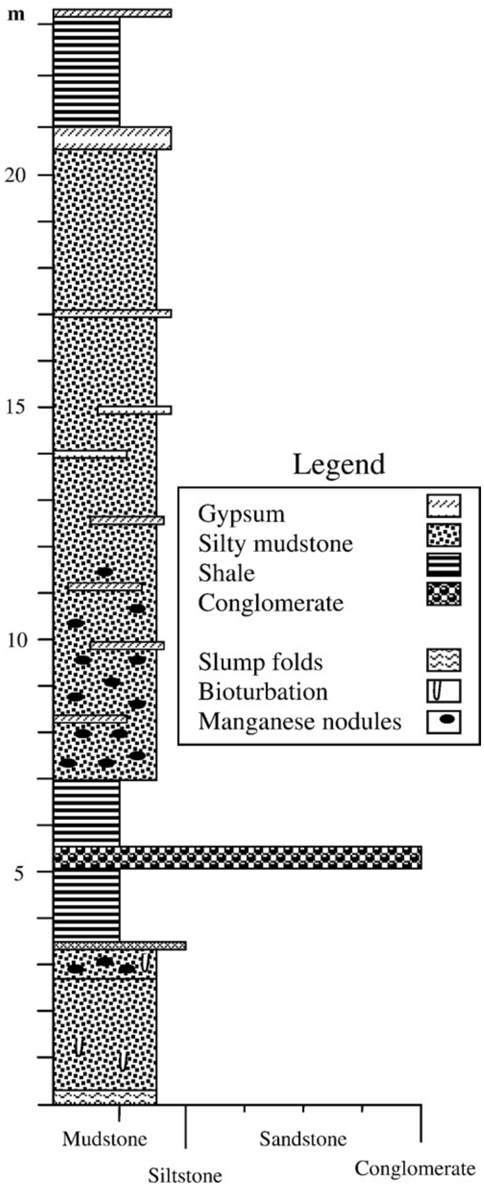

Fig. 2. Measured stratigraphic column at Playa Chorrillos, indicating the stratigraphic position of the nodule-hosting units.

The second (upper) nodule unit is a more resistant, cliff-forming interval consisting of silty shale with numerous thin, irregular gypsum bands and veins. This unit is 14 m thick and contains many manganese nodules at its base. The majority of the nodules display typical botryoidal shapes, but most have been oxidized to limonite. About 10 m from the basal contact, a break in sedimentation is formed by a 10 cm thick, irregular but laterally continuous, brownish grey gypsum bed showing small fibrous crystals (selenite) growing vertical to the bedding. The top of the unit is formed by a 40 cm thick gypsum bed enclosing many calcareous concretions, which are up to 3 m long, parallel to the bedding. The gypsiferous unit is overlain by 220 cm of reddish, silty shale capped by a 10 cm thick gypsum bed.

The benthonic foraminifers *Siphonodosaria advena*, *Cassidulina laevigata*, *Bolivina sinuate* and *Bolivina pyrula* were identified by us in the nodule-bearing interval. The preferred depth range of *S. advena* and *B. pyrula* is between 500 and 1500 m, whereas *C. laevigata* and *B. sinuata* are normally encountered at depths of 200 to 500 m. A median to upper bathial depth, i.e. the upper continental slope, can therefore be assumed. This coincides with the presence of fine-grained, massive sandstones showing occasional small-scale trough cross-lamination and fluid escape structures, fining upward into shales. These may represent partial Bouma cycles and deposition by turbidity currents. The thin pebble bands and lenses within the mudstones are interpreted as minor debris flow deposits.

Achurra (2004), based on palaeontological, stratigraphic and sedimentological analysis, concluded that tectonic subsidence of about 1000 m took place between 9 and 8 Ma, followed by uplift of the same order from about 8 to 7 Ma. $^{87}Sr/^{86}Sr$ dating of the stratigraphic units underlying and overlying the nodule-bearing interval at 9.0 ± 1.0 Ma and 6.8 ± 0.8 Ma, respectively, thus indicates that deposition of the lower nodule beds probably occurred at around 8 Ma when this part of the sea floor reached its lowest elevation, whereas the upper nodules beds may reflect somewhat shallower water during the subsequent uplift cycle. An analogue situation is shown in Fig. 4, which depicts the present position of the Bahía Inglesa Basin on a topographic-bathymetric representation of the area (from Comte et al., 2002), as well as the presence of basins on the continental slope (one of which one is outlined). Of interest here are the topographic highs between the Bahía Inglesa Basin and the continental slope, which may have caused local restrictive conditions during periods of uplift.

The Sr-dates also allow the sedimentation rate of the nodule-bearing stratigraphic unit, which has a total thickness of 57 m, to be calculated at around 0.026 mm/year. Compared with the much lower sediment accumulation rate of 0.001–0.003 mm/year associated with deep-sea nodules (Lisitzin, 1972), a more proximal environment is indicated. The presence of manganese nodules in an area with such a high overall sedimentation rate suggests intermittent periods of slow deposition between turbidity currents, or alternatively winnowing by bottom or contour currents.

Considering the presence of slumped beds, possible Bouma cycles, a higher sedimentation rate than that of deep-sea basins, and the depths indicated by benthic foraminifers, an environment varying from the upper continental slope (lower nodule zone) to outer shelf (upper zone) is very likely. This is strongly supported by the presence of a submarine palaeocanyon with debris flow deposits occurring in the stratigraphic section below the nodule-bearing units.

A possible objection to this environment may be the presence of abundant gypsum in the upper nodule-bearing unit, which is normally precipitated from standing bodies of saline water by evaporation. However, Siesser and Rogers (1976) describe the presence of authigenic gypsum together with manganese-rich, granular masses of authigenic pyrite in silty clays at water depths between 632 and 900 m on the Namibian continental slope. These authors attribute the gypsum to the upwelling of cold, nutrient-enriched waters supporting a large population of plankton, the death and decomposition of which consumed oxygen and created a belt of anaerobic sedimentation on the continental slope during a late Miocene–early Pliocene regression. Anaerobic bacteria reduced SO_4 dissolved in the sea water, forming H_2S that reacted with iron

Fig. 3. a) Spherical, botryoidal manganese nodule within basal zone. b) Manganese nodule replacing *Ophiomorpha* burrow, indicating a diagenetic origin.

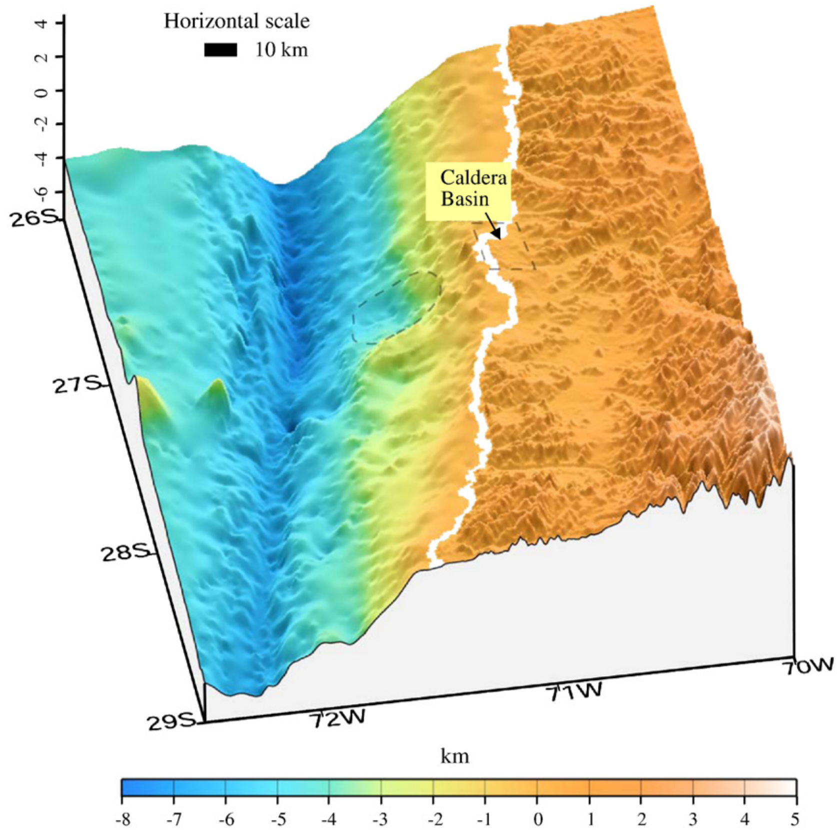

Fig. 4. Topography and bathymetry of the study area (after Comte et al., 2002). Note present-day mid-slope basin (delineated), which may represent an analogue of the Bahía Inglesa Basin during periods of maximum subsidence, as well as topographic highs partially separating the basin from the continental slope.

minerals in the sediment to form FeS. This strongly reducing, low pH environment became saturated with calcium obtained by the dissolution of calcareous organisms, precipitating gypsum when the product of the calcium and SO_4 concentrations exceeded the gypsum solubility product. In the Bahía Inglesa Formation, intensive upwelling is supported by the presence of phosphate minerals and cetaceous fossil bones in some horizons. Local, somewhat restricted conditions created by topographic highs on the seaward side of the

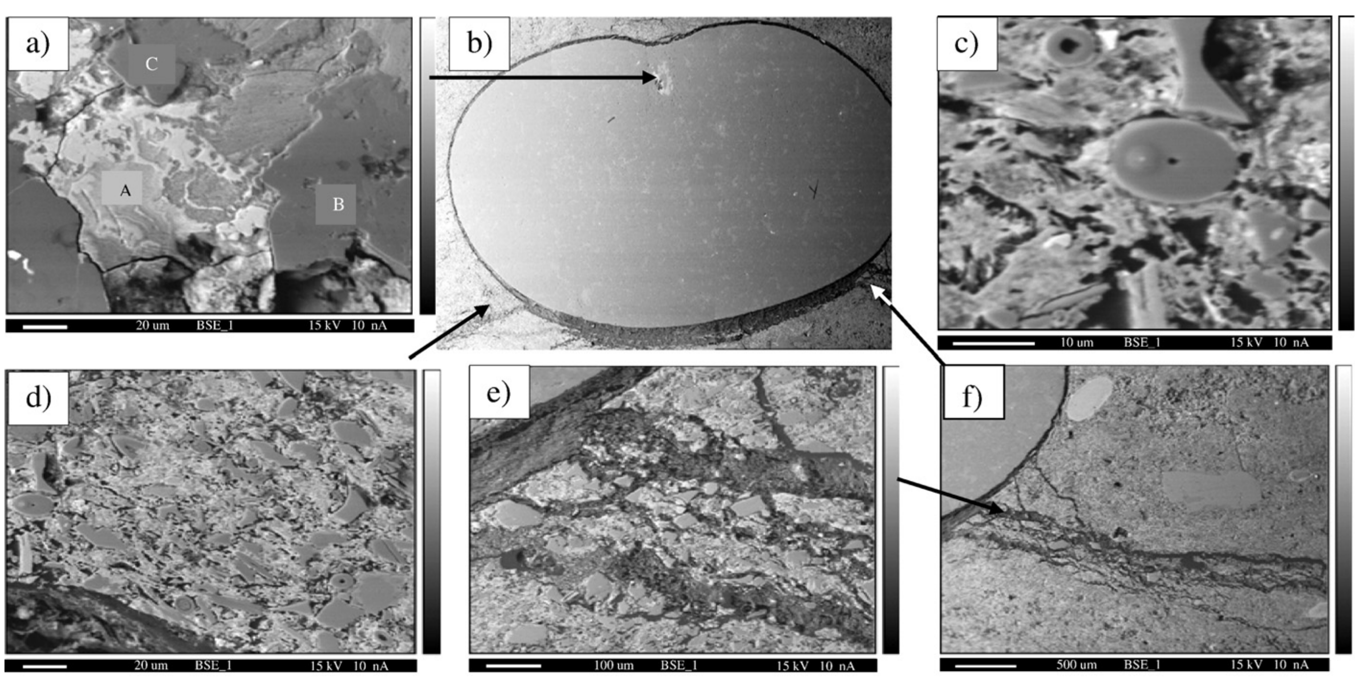

Fig. 5. Manganese nodule under SEM. a) Details of nucleus, showing intergrown manganese oxides (A), plagioclase (B), and quartz (C). b) Ellipsoidal nucleus surrounded by organic carbon. c) Diatom within outer nodule. d) Outer nodule consisting of silicate minerals (dark grey) enclosed in a matrix of amorphous manganese oxides (light grey). e) and f) Braided carbon veinlets connecting internal carbon layer with nodule exterior.

Table 3
X-ray diffraction of manganese nodules from the Bahía Inglesa Formation.

Sample	Albite	Quartz	Micas	Cryptomelane	Pyrolusite	Todorokite	Dolomite
Cal-75/4	+++	++	+	Traces			
Cal-118/1						*	
Cal-118/2						*	
Cal-118/3						*	*
Cho-1-6/1	*	*		*	*	Traces	
Cho-1-6/2	*	*				*	
Cho-1-6/3	*	*	*				*
Cho-1-6/4	*	*				*	
Cho-1-6/5	*	*				*	*
Cho-1-6/6	*	*				*	*

x = indications; * = present, content unknown; + = scarce; ++ = common; +++ = very common.

basin may also have contributed to gypsum precipitation during periods of tectonic uplift.

4. Petrography

Under SEM (Fig. 5), one of the larger nodules from the lower nodule zone shows an ellipsoidal, well-rounded nucleus composed of an association of poorly crystallized minerals including quartz, plagioclase and manganese oxides. It is surrounded by a thin (100–150 μm) layer of organic carbon associated with granular minerals. Thin, braided veinlets of carbon extending from this layer connect the nucleus with the external surface and are responsible for the deeply indented, botryoidal shape of the nodule, as they weather out more rapidly than the outer layer. The latter has a thickness of about 1.3 cm, being composed of silicate minerals such as quartz and plagioclase, together with siliceous micro-organisms including diatoms, enclosed in an amorphous matrix of manganese oxides. This layer is massive, without the thin concentric internal layers typical of many deep-sea manganese nodules, indicating a continuous accretion of minerals. According to the microscopic descriptions of Halbach et al. (1981), this coating is comparable to the massive layers of todorokite associated with early diagenetic nodules. X-ray diffraction of different manganese nodules from the Bahía Inglesa Formation (Table 3) in fact does show the presence of todorokite (Post, 1999), with a composition of $NaMn_6O_{12}.3H_2O$.

According to Nicholson (1992a,b), todorokite is rare in S_{TS} and S_{TF} nodules, but common in S_M and H_M nodules. Within the S_M group, todorokite is typical of diagenetic nodules, whereas hydrogenetic nodules are dominated by vernadite. Todorokite forming in S_{MDH} nodules is generally much depleted in Cu and Ni and enriched in Mn^{+2} and Mn^{+3}, reflecting the metal flux of suboxic, diagenetic pore water (Roy, 1992).

Samples Cal-75/4 and Cho-1-6/1 (Table 3) also yielded trace amounts of cryptomelane, in addition to common albite and quartz, some micas and traces of gypsum and amphiboles. Cryptomelane is rare in S_{TS} nodules, but is known to occur in both H_T and S_M nodules (Nicholson, 1992a,b). It may also be of diagenetic origin (Vodyanitskii et al., 2004).

The discoidal shape and botryoidal surface texture of the nodules, the fact that some of them replace *Ophiomorpha* burrows, and the dominance of todorokite together with organic carbon (suggesting a reducing environment) are all consistent with a diagenetic origin.

5. Geochemistry

Table 4 shows the geochemistry of 12 Bahía Inglesa nodules, 6 from the lower zone (Cho) and 6 from the upper zone (Cal). Because of the closed-sum problem mentioned above, we applied the traditional binary and ternary diagrams only in a preliminary way to analyze the geochemistry, basing our final analysis on more sophisticated techniques.

Our preliminary analyses proved to be inconclusive. With regard to single elements, the Zn content of the Bahía Inglesa nodules partly overlaps that of S_{MD} nodules, while the nodules from the upper zone have a higher mean concentration (0.123 wt.%) than the lower zone (0.023 wt.%). Higher concentrations of Zn are typical of hemipelagic zones and reflect enrichment of marine plankton (Martin and Knauer, 1973), which in this case may be related to marine upwelling. The average Cu content of the Bahía Inglesa nodules is 0.005 wt.%, which is less than that of S_{MD} nodules and coincides better with S_{TF} and S_{MS} nodules. This may be partly due to the relative scarcity of siliceous diatoms and radiolarians within these deposits, which are important carriers of Cu (Halbach et al., 1979; Marchig et al., 1979). As these organisms are normally less abundant above the CCD, the low Cu may thus provide additional support for an upper continental slope to shelf environment rather than deep water.

The average Mn/Fe ratio of the lower nodule zone (5.47) is lower than that of the upper zone (9.35), the former coinciding with hydrogenetic and diagenetic oxic S_{MD} nodules and the latter tending towards diagenetic suboxic types. In contrast, the Co/(Ni + Cu) ratio (0.23) compares better with S_{ME} than S_{MD} nodules, whereas the average Fe/(Ni + Cu) ratio (46.6) is also much higher than the average

Table 4
Geochemistry of 12 Bahía Inglesa nodules (values in wt.%).

Sample	Si	Al	Mn	Fe	Mg	Na	Ca	K	P	Ni	Cu	Co	Zn
Cal-118/1	14.544	3.973	27.216	2.154	2.864	2.203	1.279	1.312	0.249	0.360	0.003	0.027	0.310
Cal-118/2	18.607	5.467	18.394	3.098	2.406	2.278	1.294	1.486	0.157	0.450	0.004	0.055	0.260
Cal1-18/3	14.913	4.276	13.856	1.923	4.577	1.743	6.011	1.229	0.157	0.096	0.005	0.013	0.073
C-122	18.289	4.223	27.216	1.511	0.657	1.862	1.579	1.503	0.070	0.004	0.046	0.030	0.008
Cal-75/2		5.329	11.300	1.853	3.124		2.523			0.043	0.006	0.005	0.036
Cal-75/3		5.271	11.796	1.895	3.111		2.501			0.041	0.005	0.005	0.048
Cho-1-6/1	18.544	5.203	9.348	1.976	2.329	2.315	3.015	1.580	0.333	0.041	0.003	0.007	0.039
Cho-1-6/2	16.402	5.093	11.192	3.644	3.994	2.200	3.590	1.290	0.117	0.020	0.004	0.008	0.019
Cho-1-6/3	17.124	5.338	10.897	1.749	4.009	2.045	4.124	1.835	0.118	0.027	0.005	0.009	0.020
Cho-1-6/4	16.650	5.138	10.185	1.972	3.849	2.180	2.605	1.815	0.126	0.024	0.004	0.009	0.019
Cho-1-6/5	17.910	5.358	9.495	1.588	3.694	2.285	4.439	1.895	0.105	0.029	0.005	0.010	0.022
Cho-1-6/6	16.543	4.838	11.594	1.511	4.469	2.010	4.034	1.750	0.111	0.027	0.004	0.008	0.022

Table 5
Mn-nodule geochemical data used for the MDA and ANN analyses.

Type	Environment	Mn	Fe	Co	Zn	Ni	Cu	Reference
S_{MDS}	h	23.010	11.600	0.300	0.130	0.700	0.440	Halbach et al. (1981)
		22.100	9.250	0.420	0.088	0.870	0.413	Dymond et al. (1984)
		27.200	7.010	0.327	0.146	1.440	0.857	Dymond et al. (1984)
		27.700	7.330	0.334	0.134	1.260	0.843	Dymond et al. (1984)
		29.800	7.060	0.335	0.161	1.590	1.007	Dymond et al. (1984)
		28.800	8.140	0.402	0.150	1.320	0.810	Dymond et al. (1984)
		26.100	3.600	0.140	0.220	1.160	0.810	Halbach et al. (1979)
	d/h	22.410	7.400	0.190	0.110	1.060	0.730	Halbach et al. (1981)
		21.500	6.100	0.180	0.160	1.040	0.690	Halbach et al. (1981)
		24.700	5.740	0.170	0.170	1.210	1.090	Halbach et al. (1981)
		30.500	4.140	0.211	0.195	1.620	1.230	Dymond et al. (1984)
		27.800	5.310	0.224	0.165	1.490	1.162	Dymond et al. (1984)
		28.800	5.040	0.223	0.160	1.590	1.102	Dymond et al. (1984)
		29.300	4.510	0.212	0.170	1.440	1.257	Dymond et al. (1984)
		29.000	4.990	0.202	0.157	1.460	1.192	Dymond et al. (1984)
	d	27.100	5.100	0.130	0.240	1.430	0.930	Halbach et al. (1981)
		27.880	4.300	0.200	0.280	1.250	1.230	Halbach et al. (1981)
		28.000	5.310	0.284	0.164	1.700	1.070	Dymond et al. (1984)
		32.300	3.570	0.180	0.240	1.840	1.496	Dymond et al. (1984)
		31.900	3.720	0.231	0.216	2.010	1.375	Dymond et al. (1984)
		31.500	5.150	0.260	0.220	1.480	1.160	Dymond et al. (1984)
		32.300	3.620	0.261	0.215	1.840	1.248	Dymond et al. (1984)
S_{MDR}	h	16.300	15.520	0.349	0.060	0.460	0.220	Dymond et al. (1984)
		16.900	17.470	0.330	0.060	0.530	0.328	Dymond et al. (1984)
		14.100	19.100	0.296	0.047	0.280	0.183	Dymond et al. (1984)
		17.400	16.440	0.367	0.057	0.490	0.248	Dymond et al. (1984)
	d/h	21.300	11.100	0.320	0.081	0.820	0.500	Dymond et al. (1984)
		21.400	10.370	0.283	0.091	0.990	0.590	Dymond et al. (1984)
		19.300	12.870	0.308	0.071	0.710	0.434	Dymond et al. (1984)
		18.400	11.860	0.290	0.062	0.680	0.376	Dymond et al. (1984)
	d	20.000	11.450	0.257	0.074	0.750	0.569	Halbach et al. (1981)
		20.100	12.290	0.224	0.074	0.880	0.500	Halbach et al. (1981)
		21.800	11.420	0.219	0.084	1.050	0.680	Halbach et al. (1981)
		20.900	11.650	0.224	0.081	0.870	0.561	Halbach et al. (1981)
S_{MDH}	h	32.100	5.700	0.029	0.207	0.908	0.500	Dymond et al. (1984)
		34.800	3.950	0.023	0.231	0.805	0.506	Dymond et al. (1984)
		35.000	4.450	0.028	0.232	0.810	0.532	Dymond et al. (1984)
		31.600	5.350	0.037	0.180	0.853	0.566	Dymond et al. (1984)
		32.000	4.370	0.024	0.187	0.918	0.551	Dymond et al. (1984)
		35.100	3.520	0.022	0.270	0.906	0.495	Dymond et al. (1984)
		35.600	4.650	0.024	0.237	0.888	0.490	Dymond et al. (1984)
		34.100	3.970	0.021	0.243	0.932	0.464	Dymond et al. (1984)
		33.800	5.240	0.029	0.258	0.821	0.391	Dymond et al. (1984)
		40.900	1.570	0.009	0.271	0.483	0.260	Dymond et al. (1984)
		40.200	2.340	0.014	0.258	0.581	0.296	Dymond et al. (1984)
		37.300	2.540	0.013	0.266	0.732	0.345	Dymond et al. (1984)
		36.900	3.300	0.019	0.287	0.849	0.382	Dymond et al. (1984)
		40.100	2.130	0.015	0.248	0.642	0.275	Dymond et al. (1984)
		35.500	4.270	0.026	0.253	0.834	0.522	Dymond et al. (1984)
		43.500	2.110	0.014	0.154	0.532	0.176	Dymond et al. (1984)
	d/h	35.300	3.900	0.023	0.209	0.812	0.485	Dymond et al. (1984)
		36.000	3.550	0.021	0.227	0.841	0.518	Dymond et al. (1984)
		34.100	4.300	0.026	0.254	0.869	0.553	Dymond et al. (1984)
		33.800	4.320	0.029	0.203	0.806	0.531	Dymond et al. (1984)
		37.200	3.840	0.022	0.203	0.830	0.446	Dymond et al. (1984)
		38.800	3.750	0.020	0.239	0.954	0.417	Dymond et al. (1984)
		36.400	3.840	0.021	0.213	0.846	0.427	Dymond et al. (1984)
		38.200	3.100	0.019	0.231	0.826	0.418	Dymond et al. (1984)
		38.500	3.010	0.018	0.266	0.798	0.385	Dymond et al. (1984)
		42.700	1.110	0.009	0.205	0.406	0.186	Dymond et al. (1984)
		39.800	2.020	0.015	0.252	0.585	0.342	Dymond et al. (1984)
		39.000	3.270	0.019	0.224	0.798	0.397	Dymond et al. (1984)
		39.800	2.740	0.017	0.213	0.634	0.298	Dymond et al. (1984)
		36.600	3.770	0.021	0.216	0.774	0.421	Dymond et al. (1984)
		39.500	3.050	0.016	0.227	0.727	0.336	Dymond et al. (1984)
		37.600	3.670	0.021	0.212	0.776	0.355	Dymond et al. (1984)
		40.800	2.690	0.015	0.202	0.706	0.379	Dymond et al. (1984)
	d	45.300	0.650	0.004	0.157	0.299	0.096	Dymond et al. (1984)
		43.900	0.690	0.005	0.218	0.483	0.176	Dymond et al. (1984)
		40.400	2.520	0.015	0.258	0.593	0.315	Dymond et al. (1984)
		41.400	1.200	0.010	0.358	0.809	0.299	Dymond et al. (1984)
		44.200	0.720	0.004	0.195	0.527	0.157	Dymond et al. (1984)
		42.800	0.910	0.008	0.223	0.731	0.178	Dymond et al. (1984)
		43.100	2.010	0.012	0.269	0.611	0.275	Dymond et al. (1984)
		46.200	1.200	0.006	0.139	0.388	0.110	Dymond et al. (1984)

Table 5 (*continued*)

Type	Environment	Mn	Fe	Co	Zn	Ni	Cu	Reference
S_{MDH}	d	46.700	0.710	0.005	0.128	0.373	0.098	Dymond et al. (1984)
		45.500	0.910	0.007	0.303	0.669	0.221	Dymond et al. (1984)
		41.300	1.180	0.006	0.274	0.326	0.172	Dymond et al. (1984)
		41.900	1.800	0.013	0.190	0.510	0.235	Dymond et al. (1984)
		46.900	1.790	0.009	0.145	0.409	0.122	Dymond et al. (1984)
		44.300	0.830	0.007	0.215	0.413	0.165	Dymond et al. (1984)
		43.800	1.100	0.008	0.171	0.436	0.137	Dymond et al. (1984)
		37.900	2.100	0.013	0.241	0.611	0.219	Dymond et al. (1984)
S_{ME}		14.030	22.470	0.016	0.008	0.075	0.005	Manheim (1965)
		9.900	22.780	0.006	0.014	0.005	0.002	Sevast´yanov (1967)
S_{TF}		13.680	39.690	0.014	0.022	0.003	0.000	Williams and Bowen (1992)
		11.170	39.690	0.010	0.015	0.003	0.000	Williams and Bowen (1992)
		19.190	34.020	0.013	0.011	0.006	0.001	Williams and Bowen (1992)
		19.200	33.620	0.008	0.010	0.006	0.001	Williams and Bowen (1992)
		4.730	35.630	0.008	0.005	0.004	0.004	Sweden
		7.250	15.140	0.003	0.111	0.003	0.001	UK
		9.150	20.760	0.012	0.032	0.024	0.003	Michigan

for S_{MD} nodules (5.5). These apparently conflicting results either indicate that the diagrams traditionally used in analyzing Mn-nodule geochemistry are unreliable in distinguishing between different nodule types, or that the Bahía Inglesa nodules simply do not conform to the present classification scheme.

In order to investigate this further, we analyzed the geochemical characteristics of different types of nodules using multiple discriminant analysis (MDA) as well as a new technique, artificial neural networks (ANN). To establish whether these methods are better able to determine palaeoenvironments from geochemical data, we studied a literature-derived geochemical dataset that comprises 92 manganese nodules with concentration data (wt.%) for six elements (Mn, Fe, Co, Zn, Ni and Cu), which are those most commonly reported in publications on ferromanganese nodules.

Because diagenetic (designated by the symbol d) and hydrogenetic (h) nodules occurring within the same environment have different geochemical signatures, they were treated separately. In the case of mixed diagenetic/hydrogenetic (d/h) nodules, the geochemistry of nodule bottoms are sometimes reported separate from the tops (e.g. Dymond et al., 1984). In these cases the bottoms were considered to be diagenetic and the tops as hydrogenetic. Where bulk ratios of mixed hydrogenetic and diagenetic nodules were reported, these were considered as a special, intermediate class (d/h).

The geochemical data were grouped into four main nodule types including 22 S_{MDS}-type nodules (S_{MDSh}, $S_{MDSd/h}$ and S_{MDSd} types), 12 S_{MDR}-type nodules (S_{MDRh}, $S_{MDRd/h}$ and S_{MDRd} types), 49 S_{MDH}-type nodules (S_{MDHh}, $S_{MDHd/h}$ and S_{MDHd} types), and 9 S_{TF-ME}-type nodules (S_{TF} and S_{ME} types; Table 5). Prior to both the MDA and ANN analyses, the original variables (Mn, Fe, Co, Zn, Ni and Cu) were normalized using the centered log-ratio (CLR) transformation instead of the additive log-ratio transformation (ALR). CLR transformation allows the use of conventional statistics based on Euclidian distance measures, whereas ALR employs a common denominator and therefore induces strong intercorrelation of (log)-ratioed variables (G.J. Weltje, pers. comm., 2009). Any undesirable properties derived from the closure of the compositional data could thus be eliminated.

5.1. MDA analysis

MDA is a multivariable statistical technique that is used to visualize first-order (linear) differences between groups of samples. It is a "supervised" technique that will not distinguish natural groups within sets of data, as it relies upon prior knowledge of the groupings. MDA creates a new function from the independent variables, which is defined such that it provides the maximum separation between the means of the pre-defined groups of the dataset. A second function is then computed uncorrelated with the first, followed by calculating a third function uncorrelated with the first two. This iterative process continues until the number of calculated functions equals the lesser of $g-1$ (where g is the number of pre-defined groups) or the number of independent variables. This technique is sensitive to outliers, assuming multivariate normality and that the variability within the pre-defined groups is similar for the independent variables (Le Maitre, 1982).

The MDA analysis of the nodule dataset resulted in a set of discriminant functions. The unstandardized coefficients of those discriminant functions associated with the two main eigenvalues (FI and FII) are shown in Table 6. Because of the CLR transformation, the variables correspond to the natural logarithm value of the elements Mn, Fe, Co, Zn, Ni and Cu. The coefficients of Table 6 indicate that the FI function is sensitive to the concentrations of Co and Fe. Consequently, in the FI vs. FII diagram (Fig. 6) the S_{MDR} and S_{MDS} nodules cluster at higher FI values than the S_{MDH}, S_{TF} and S_{ME} nodules, in agreement with their comparatively higher Co concentrations (Co averages of 0.29, 0.25, 0.02, 0.01, 0.01 and 0.01 wt.%, respectively). In contrast, the negatively scored concentration of Fe (Table 6) seems to control subtler differences in terms of FI, such as those observed between the S_{MDS} and S_{MDR} clusters (Fe averages of 5.8 and 13.5 wt.%, respectively; Fig. 6).

The coefficients of Table 6 indicate that FII is mainly controlled by the concentration of Mn and, to a lesser extent, by the concentration of Co. Accordingly, because of their marked enrichment in Mn, the S_{MDH} nodules (average Mn concentration of 39.1%) are highly differentiated in terms of FII from the S_{MDS}, S_{MDR}, S_{TF} and S_{ME}-type nodules (average Mn concentrations of 27.7, 19.0, 12.1 and 12.0%, respectively; Fig. 6).

For both the FI and FII functions, the coefficients associated with the concentration of Zn are comparatively low (Table 6). This suggests that the concentration of Zn is not a relevant variable to discriminate between the S_{MDS}, S_{MDR}, S_{MDH}, S_{TF} and S_{ME}-type nodules.

Close examination of the data in Table 5 shows that for the S_{MDR}, S_{MDS} and S_{MDH}-type nodules there is a net chemical change from hydrogenetic to diagenetic conditions. For both the S_{MDR} and S_{MDS}-

Table 6
Unstandardized coefficients of the discriminant functions FI and FII associated with the MDA technique.

Variable	FI	FII
Ln (Mn)	0.115	0.770
Ln (Fe)	−0.622	0.299
Ln (Co)	0.690	−0.490
Ln (Zn)	0.033	0.088
Ln (Ni)	−0.269	0.037
Ln (Cu)	0.226	0.262
Constant	2.989	−4.055

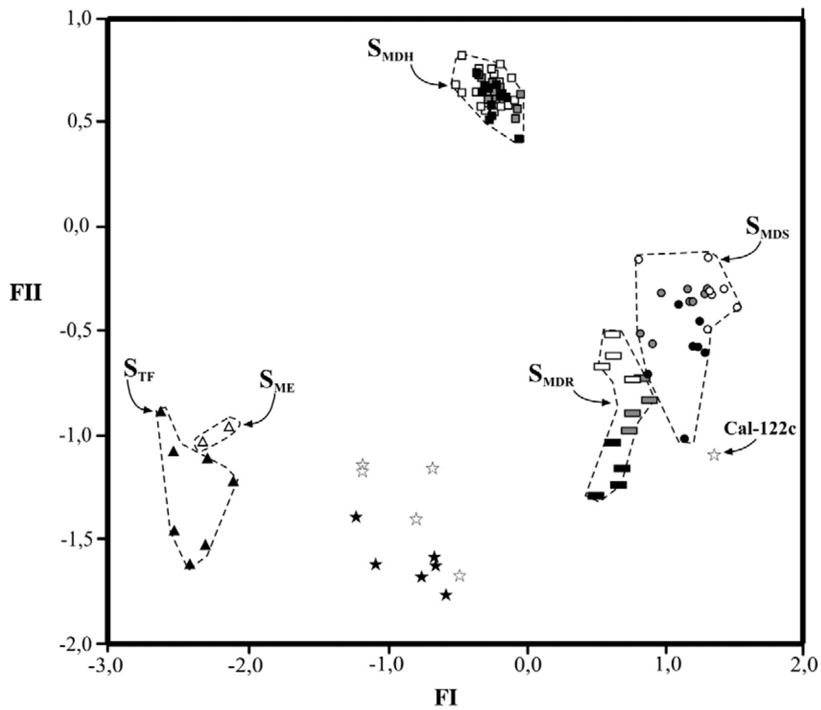

Fig. 6. FI vs. FII discriminant functions diagram, resulting from MDA analysis of the Mn-nodule dataset, using the centered log-ratio normalized values of the original variables Mn, Fe, Co, Zn, Ni and Cu. The different Mn-nodule types are indicated in: rectangles — S_{MDR}-type; circles — S_{MDS}-type; black triangles — S_{TF}-type; white triangles — S_{ME}-type; squares — S_{MDH}-type. For the S_{MDR}, S_{MDS} and S_{MDH}-nodule types the colour indicates the environmental conditions of each sample, comprising: diagenetic (white), diagenetic/hydrogenetic (grey) and hydrogenetic (black) nodules. White stars: Mn-nodule Cal samples of Bahía Inglesa Formation. Black stars: Mn-nodule Cho samples of Bahía Inglesa Formation.

type nodules the last chemical change is coincident with: a) an increase in the average content of Ni (S_{MDR}: 0.44 to 0.89 wt.% and S_{MDS}: 1.19 to 1.65 wt.%), Mn (S_{MDR}: 16.4 to 20.7 wt.%, and S_{MDS}: 26.4 to 30.1 wt.%), Zn (S_{MDR}: 0.06 to 0.08 wt.%, and S_{MDS}: 0.15 to 0.23 wt.%) and Cu (S_{MDR}: 0.24 to 0.58 wt.%, and S_{MDS}: 0.74 to 1.22 wt.%); b) a decrease in the average content of Fe (S_{MDR}: 17.1 to 11.7 wt.% and S_{MDS}: 7.7 to 4.4 wt.%) and Co (S_{MDR}: 0.34 to 0.23 wt.% and S_{MDS}: 0.32 to 0.22 wt.%). In particular, for both the S_{MDR} and S_{MDS}-type nodules, the hydrogenetic-diagenetic chemical change coincides with roughly linear trends of increasing FII values (Fig. 6). This feature is highly likely to be controlled by the hydrogenetic to diagenetic increase in Mn concentrations of the S_{MDR} and S_{MDS}-type nodules described above. In turn, for the S_{MDH}-type nodules the hydrogenetic-diagenetic chemical change coincides with an increase in the average content of Mn (36.2 to 43.5 wt.%) coupled with a decrease in the average content of Ni (0.78 to 0.51 wt.%), Fe (3.72 to 1.27 wt.%), Co (0.02 to 0.01 wt.%) and Cu (0.42 to 0.19 wt.%). As both Fe and Cu are associated with positive FII factors (Table 6), for the S_{MDH}-type nodules the effect of increasing hydrogenetic to diagenetic Mn concentrations is lessened by the associated decrease in the Fe and Cu concentrations. Therefore, the hydrogenetic and diagenetic S_{MDH}-type nodules are not clearly differentiated in terms of FII (Fig. 6).

In the FI vs. FII diagram most of the Mn-nodule samples of the Bahía Inglesa Formation are clustered in a restricted area, in an intermediate position with respect to the other Mn-nodule clusters (Fig. 6). This indicates that the MDA analysis is inconclusive with respect to the class of the Bahía Inglesa samples. However, in broad terms the Bahía Inglesa nodules display a trend of increasing FII values from the Cho to the Cal samples (Fig. 6). This suggests increasing diagenetic conditions from the lower to the upper nodule zone.

5.2. ANN analysis

Artificial neural networks (ANN) provide a non-linear, rapid and robust tool for analyzing multivariate geochemical data. By using ANN both for clustering and non-linear projecting of data onto a lower dimensional display (visualization), relevant geochemical information can be exhibited in a maximally concentrated form. ANN has been successfully tested on geochemical analysis to visualize geochemical source signatures in different materials ranging from volcanic to sedimentary rocks (Lacassie et al., 2004; Lacassie et al., 2006). Here we use an extension of the self-organizing map network or SOM (Kohonen, 1995), to analyze the 6-dimensional nodule dataset (using 6 input variables associated with Mn, Fe, Co, Cu, Ni, and Zn) and to project it onto 2- and 3-dimensional representations where the information most relevant to the clustering task is found through visual inspection.

In this case, the data analyzed with the ANN technique included the CLR-normalized data of both the literature-derived nodules and the Bahia Inglesa datasets. This “enlarged” nodule dataset was used for training the ANN. During the training phase the ANN learns from the data, i.e. their nodes become specifically tuned to the patterns or classes of the enlarged nodule dataset. This learning process is unsupervised, therefore no prior knowledge of the groupings or nodule types is used. After the learning process, the relevant information of the enlarged nodule dataset is projected onto a 2-dimensional array of 9 interconnected units or nodes (ANN map; Fig. 7a). Each node groups Mn-nodule samples with very similar geochemical signatures. Thus, a class can be assigned to each node according to the predominant Mn-nodule type of the associated nodule samples. In this case, the nodes associated with the same class are schematically grouped by dotted lines (Fig. 7). As the ANN map preserves the topology (Kohonen, 1995), the cluster structure of the enlarged nodule dataset is maintained and can be discovered by visualization of the ANN map. The results show that the ANN map models the Mn-nodule dataset as five different groups or clusters, shown on the 2-dimensional and 3-dimensional maps as five distinct areas (Fig. 7a, b and c). Four of these areas are associated with depositional environments previously used in Mn-nodule classification (S_{MDS}, S_{MDR}, S_{MDH} and S_{TF}–S_{ME}), whereas a fifth area is associated

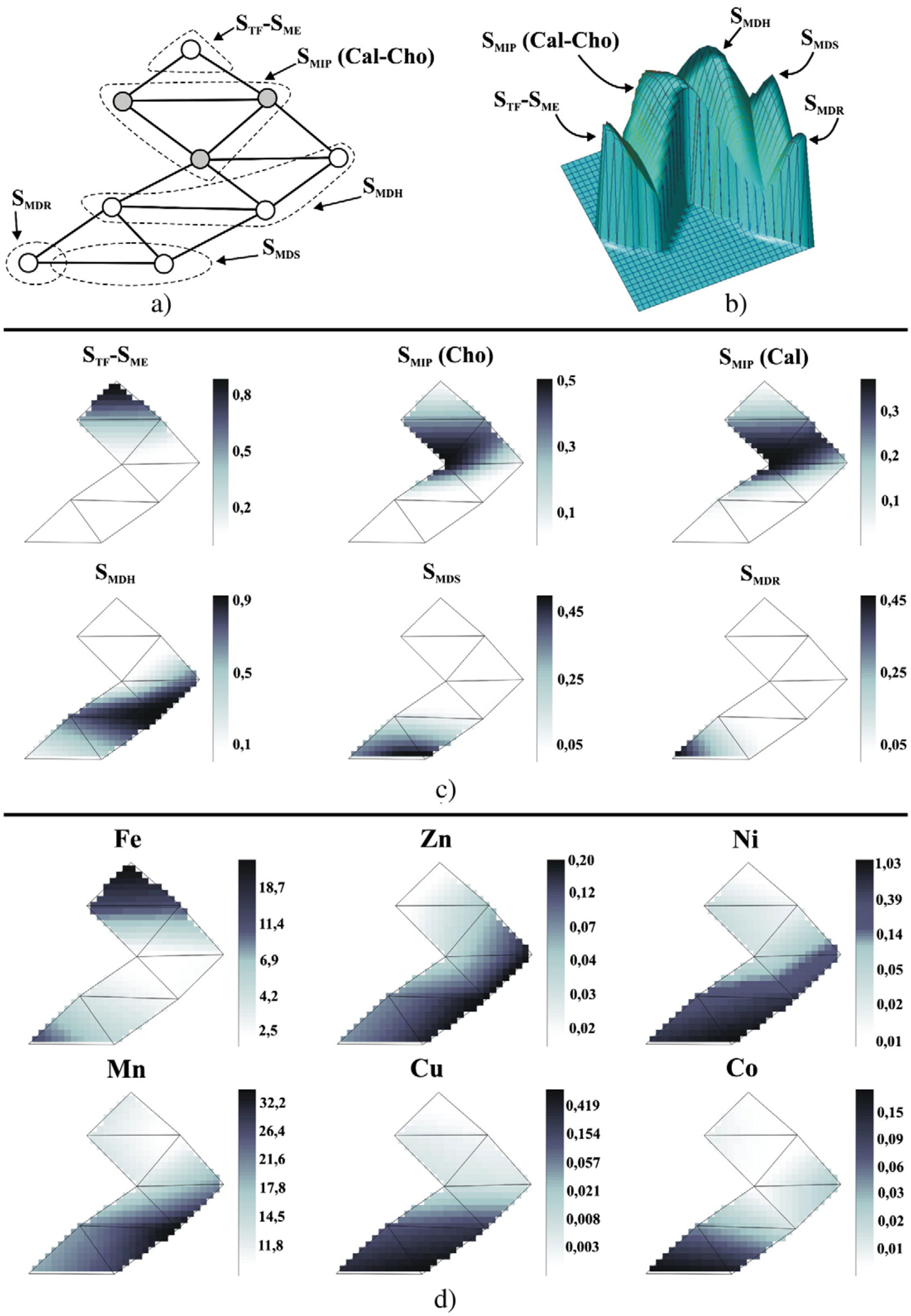

Fig. 7. See main text for an explanation of this figure. Visualization of posterior probabilities and input variable distributions for a 9-node ANN map trained with the enlarged nodule dataset, which includes the CLR-normalized Mn, Fe, Co, Zn, Ni and Cu values of both the Mn-nodule (extracted from the literature) and the Bahia Inglesa datasets. (a) ANN map structure. The nodes (circles) are schematically grouped by dotted lines according to their class. The grey circles correspond to the nodes with which the Mn-nodule samples of the Bahía Inglesa Formation (Cal and Cho samples) are associated after the ANN classification. (b) Three-dimensional and (c) two-dimensional visualization of the posterior probability distributions. S_{MDR}: supergene, deep marine (red, pelagic clay); S_{MDS}: supergene, deep marine (siliceous, pelagic ooze); S_{MDH}: supergene, deep marine (hemipelagic clay); S_{TF}: supergene, terrestrial (freshwater lakes and streams); S_{ME}: supergene, marine (epeiric seas or restricted basins); S_{MIP}: supergene, intermediate marine (partially restricted basins = Cal–Cho Bahía Inglesa samples). All five classes include the hydrogenic and diagenetic types. The posterior probability values are shown by the grey-scale axes on the right. (d) Two-dimensional visualization of the distributions of the input variables. The scales on the right are logarithmic, thus only the argument (element concentrations) are indicated. The distributions of each variable can easily be compared visually with that of the posterior probabilities, and with each other. (For interpretation of the references to colour in this figure legend, the reader is referred to the web version of this article.)

with the Bahia Inglesa samples (Cal and Cho; Fig. 7a, b and c). The ANN_map also enables two-dimensional visualization of the distributions of the input variables, which in this case correspond to the natural logarithm value of the elements Mn, Fe, Co, Zn, Ni and Cu (Fig. 7d). The scales on the right are logarithmic, thus only the argument (element concentrations) is indicated. The cluster structure of the dataset (Fig. 7a, b and c) can be easily compared with the distribution of the geochemical variables and with each other. Visual inspection of the ANN maps shows clear geochemical contrasts and affinities among the five nodule-related clusters:

- Zn and Ni, and to a lesser extent, Mn, Cu and Co are closely correlated and increase systematically from S_{TF}–S_{ME} through S_{MDS}-type nodules.
- Fe is uncorrelated with the other elements.
- S_{MDH}-type nodules are characterized by high Zn and low Fe concentrations. Thus, a high to very high Zn/Fe ratio is expected to be a discriminant characteristic of this nodule type.
- S_{TF} and S_{ME}-type nodules are characterized by low concentrations of Zn, Ni, Mn, Cu and Co, coupled with high concentrations of Fe. Therefore, low to very low Zn/Fe, Ni/Fe, Co/Fe, Cu/Fe, and Mn/Fe ratios are expected to be discriminant characteristics of these nodule types.
- High Co concentrations are typical of the S_{MDS} and S_{MDR}-type nodules. However, the S_{MDS}-type nodules are also characterized by high concentrations of Ni and Cu.
- The Mn-nodules of Bahia Inglesa (Cal and Cho samples) define a single Cal–Cho cluster located in an intermediate position between the S_{TF}–S_{ME} and the S_{MDH} clusters. This indicates that, in broad terms, the Cal and Cho nodules present a similar chemical signature that is different from the chemical signatures of the S_{MDS}, S_{MDR}, S_{MDH}, S_{TF} or S_{ME}-type nodules. This is in agreement with the results of the MDA analysis, which also suggests that the Mn-nodules of Bahia Inglesa present a geochemical signature different from the S_{MDS}, S_{MDR}, S_{MDH}, S_{TF} or S_{ME}-type nodules.
- The topological proximity between the Cal–Cho, S_{TF}–S_{ME} and the S_{MDH} clusters of the ANN map (Fig. 7), suggests that the Mn-nodules of Bahia Inglesa present a chemical composition intermediate between the compositions of the S_{MDH} and S_{TF}–S_{ME}-type nodules. In particular, the low Mn, Ni and Cu average concentrations of the Bahia Inglesa nodules (14.4, 0.097 and 0.008 wt.%, respectively) are similar to the coupled S_{TF}–S_{ME} averages (12.0, 0.014 and 0.002 wt.%, respectively). In contrast, the Fe average concentration of the Bahia Inglesa nodules (2.07 wt.%) is markedly lower than the S_{TF}–S_{ME} coupled average (29.31 wt.%), although it is very similar to the S_{MDH} Fe average concentration (2.77 wt.%), whereas the Co average concentrations of both the Bahía Inglesa and the S_{MDH} nodules are almost equivalent (0.015 and 0.017 wt.%, respectively). Only in terms of the average Zn concentrations do the Bahía Inglesa nodules differ from their S_{TF}–S_{ME} and S_{MDH} counterparts (0.073, 0.025 and 0.226 wt.%, respectively), and are similar to the S_{MDR} nodules (0.070 wt.%).

6. Conclusions

- Micropalaeontological and sedimentological evidence indicate that the Bahía Inglesa nodules formed on the upper continental slope (lower nodule zone) to outer shelf (upper nodule zone).
- The replacement of *Ophiomorpha* burrows by nodules in the lower zone indicates a diagenetic origin.
- In the case of the upper nodule zone, the abundant presence of gypsum and relatively high concentrations of Zn suggest that strong upwelling coincided with the proliferation of plankton. The environment could also have been locally more restricted because of topographic highs on the seaward side of the basin, which may have formed partial barriers after uplift.
- The nodule petrology, in particular the dominance of todorokite, suggests that they belong to the S_M group rather than S_{TS}, S_{TF} or H_M.
- The multi-component MDA analysis plots outside of the fields defined by S_{TF}, S_{ME}, S_{MDH} or S_{MDR} nodules. However, it suggests increasing diagenetic conditions from the lower to the upper nodule zone of the Bahía Inglesa Formation.
- In agreement with the results of the MDA analysis, the results of the ANN analysis suggest that the Mn-nodules of Bahía Inglesa present a distinct geochemical signature that is different from the compositions associated with the S_{MDS}, S_{MDR}, S_{MDH}, S_{TF} or S_{ME}-type nodules, being intermediate between the compositions of the S_{MDH} and the S_{TF}–S_{ME}-type nodules. This seems to indicate an environment with intermediate depth marine characteristics (continental slope to outer shelf), at times subjected to somewhat restricted conditions because of topographic highs forming partial barriers to ocean circulation. We therefore propose a new Mn-nodule class, here termed S_{MIP}: supergene, intermediate marine (partially restricted basins).

Acknowledgements

This research was funded by Project Fondecyt 1010691. J.P. Lacassie was supported by CONICYT under a post-doctoral fellowship, Fondecyt # 3060056. The statistical analysis was carried out using the GCSVIS toolbox developed by Andrew Walker, Robert Harrison and Simon Cross at the University of Sheffield. J.P. Le Roux completed part of this study as a fellow of the Hanse Institute for Advanced Study in Delmenhorst, Germany — the logistical and financial support of the Institute is greatly appreciated. We are greatly indebted to Editor Gert Jan Weltje and two anonymous reviewers for many helpful suggestions, which significantly improved this paper.

References

Achurra, L.E., 2004. Cambios del nivel del mar y evolución tectónica de la cuenca neógena de Caldera, III Región. Unpubl. M. thesis, Universidad de Chile, Santiago, 138.
Aitchison, J., 1986. The Statistics Analysis of Compositional Data. Chapman and Hall, London, UK. 416.
Armstrong-Altrin, J.S., Surendra, T., Verma, P., 2005. Critical evaluation of six tectonic setting discrimination diagrams using geochemical data of Neogene sediments from known tectonic settings. Sedimentary Geology 177, 115–129.
Audley-Charles, M.G., 1965. A geochemical study of Cretaceous ferromanganiferous sedimentary rocks from Timor. Geochimica et Cosmochimica Acta 29, 1153–1173.
Banakar, V.K., Nair, R.R., Tarkian, M., Haake, B., 1993. Neogene oceanographic variations recorded in manganese nodules from the Somali Basin. Marine Geology 110 (3–4), 393–402.
Banerjee, R., Miura, H., 2001. Distribution pattern and morphochemical relationships of managanese nodules from the Central Indian Basin. Geo-Marine Letters 21 (1), 34–41.
Banerjee, R., Roy, S., Dasgupta, S., Mukhopadhyay, S., Miura, H., 1999. Petrogenesis of ferromanganese nodules from east of the Chagos Archipelago, Central Indian Basin, Indian Ocean. Marine Geology 157 (3–4), 145–158.
Barbera, G., Lo Giudice, A., Mazzoleni, P., Pappalardo, A., 2009. Combined statistical and petrological analysis of provenance and diagenetic history of mudrocks: application to Alpine Tethydes shales (Sicily, Italy). Sedimentary Geology 213, 27–40.
Bonatti, E., Kraemer, T., Rydell, H., 1972. Classification and genesis of submarine iron–manganese deposits. In: Horn, D.R. (Ed.), Ferromanaganese Deposits on the Ocean Floor. National Science Foundation, Washington, pp. 149–166.
Bu, W.R., Shi, X.F., Peng, J.T., Qi, L., 2003. Geochemical characteristics of seamount ferromanganese nodules from mid-Pacific Ocean. Chinese Science Bulletin 48, 98–105.
Butler, J.C., 1979. Trends in ternary petrologic variation diagrams—fact or fantasy? American Mineralogist 64, 1115–1121.
Chayes, F., 1960. On correlation between variables of constant sum. Journal of Geophysical Research 65, 4185–4193.
Crerar, D., Barnes, H., 1974. Deposition of ancient nodules. Geochimica et Cosmochimica Acta 38, 279–300.
Comte, D., Haessler, H., Dorbath, L., Pardo, M., Monfret, T., Lavenu, A., Pontoise, B., Hello, Y., 2002. Seismicity and stress distribution in the Copiapó, northern Chile subduction zone using combined on- and off-shore seismic observations. Physics of the Earth and Planetary Interiors 132, 197–217.
Cronan, D.S., 1977. Deep-sea nodules: distribution and geochemistry. In: Glasby, G.P. (Ed.), Marine Manganese Deposits. Elsevier, Amsterdam, pp. 11–44.

Duff, P., 1993. Holmes´ Principles of Physical Geology, (4th edition). Chapman & Hall, London. 789.
Dymond, J., Lyle, M., Finney, B., Piper, D., Murphy, K., Conard, R., Pisias, N., 1984. Ferromanganese nodules from MANOP sites H, S, and R. Control of mineralogical and chemical composition by multiple accretionary processes. Geochimica et Cosmochimica Acta 48, 931–949.
Giresse, P., Wiewiora, A., Lacka, B., 1998. Processes of Holocene ferromanganese-coated grains (oncolites) in the nearshore shelf of Cameroon. Journal of Sedimentary Research 68 (1), 20–36.
Godoy, E., Marquardt, C., Blanco, N., 2003. Carta Caldera. Región de Atacama. Carta Geológica de Chile, Serie Geología Básica, No. 76. Servicio Nacional de Geología y Minería, Santiago. 38.
Halbach, P., Özkara, M., Rehm, E., 1977. Untersuching von Manganknollen und sedimentproben der VA 13/1. Ergebnisse der Manganknollenfahrt VA 13/1 (Zentraler Pazifischer Ozean, 1976). Fachlicher Bericht, Hannover (BGR). 35.
Halbach, P., Rehm, E., Marchig, V., 1979. Distribution of Si, Mn, Fe, Ni, Cu, Co, Zn, Pb, Mg, and Ca in grain-size fractions of sediment samples from a manganese nodule field in the Central Pacific Ocean. Marine Geology 29, 237–252.
Halbach, P., Scherlag, C., Hebisch, U., Marchig, V., 1981. Geochemical and mineralogical control of different genetic types of deep-sea nodules from the Pacific Ocean. Mineral Deposits 16, 59–84.
Hlawatsch, S., Neumann, T., Van den Berg, C.M.G., Kersten, M., Harff, J., Suess, E., 2002. Fast-growing, shallow-water ferro-manganese nodules from the western Baltic Sea: origin and modes of trace element incorporation. Marine Geology 182 (3–4), 373–387.
Hu, W.X., Jin, Z.J., Yao, S.P., Lu, X.C., Chen, Z.L., Zhang, X.J., Zhou, H.Y., 2002. Discovery of low-mature hydrocarbon in manganese nodules and ooze from the Central Pacific deep sea floor. Chinese Science Bulletin 47 (11), 939–944.
Jung, H.S., Lee, C.B., 1999. Growth of diagenetic ferromanganese nodules in an oxic deep-sea sedimentary environment, northern equatorial Pacific. Marine Geology 157 (3–4), 127–144.
Kohonen, T., 1995. Self-organising maps. In: Huang, T., Schroeder, M. (Eds.), Springer Series in Information Sciences, vol. 30. Springer-Verlag, Berlin, Germany. 362.
Lacassie, J.P., Roser, B.P., Ruiz del Solar, J., Hervé, F., 2004. Visualization of geochemical datasets by using neural networks: a novel perspective for sedimentary provenance analysis. Sedimentary Geology 165, 175–191.
Lacassie, J.P., Ruiz del Solar, J., Roser, B.P., Hervé, F., 2006. Visualization of volcanic rock geochemical data and classification with artificial neural networks. Mathematical Geology 38 (6), 697–710.
Le Maitre, R.W., 1982. Numerical Petrology: Statistical Interpretation of Numerical Data. Elsevier Science, Amsterdam. 281.
Lisitzin, A.P., 1972. Sedimentation in the World Ocean. SEPM Special Publication 17 218.
Manheim, F.T., 1965. Manganese-iron accumulations in the shallow marine environment. Narrgansett Marine Laboratory, Occasional Publ. 3, 217–276.
Marchig, V., Gundlach, H., Schnier, Ch., 1979. Verhalten von Radiolarienschalen aus dem Zentralpazifik bei der Diagenese. Geologische Rundschau 68, 1037–1053.
Marchig, V., Von Stackelberg, U., Hufnagel, H., Durn, G., 2001. Compositional changes of surface sediments and variability of manganese nodules in the Peru Basin. Deep-sea Research. Part 2. Topical Studies in Oceanography 48 (17–18), 3523–3547.
Marquardt, C., Blanco, N., Godoy, E., Lavenu, A., Ortlieb, L., Marchant, M., Guzmán, N., 2000. Estratigrafía del Cenozoico Superior en el área de Caldera (26°45′–28°S). Actas IX Congreso Geológico Chileno, Puerto Varas, vol. 2, pp. 504–508.
Martin, J.H., Knauer, G.A., 1973. The elemental composition of plankton. Geochimica et Cosmochimica Acta 37, 1639–1654.
Menard, H., Shipek, C., 1958. Surface concentrations of manganese nodules. Nature 182, 1156–1158.
Morales, E., 1984. Geografía de los Fondos Marinos del Mar Chileno. Instituto Geográfico Militar, Santiago. 206.
Nicholson, K., 1992a. Genetic types of manganese oxide deposits in Scotland: indicators of palaeo-ocean spreading rate and a Devonian geochemical mobility boundary. Economic Geology 87, 1301–1309.
Nicholson, K., 1992b. Contrasting mineralogical–geochemical signatures of manganese oxides: guides to metallogenesis. Economic Geology 87, 1253–1264.
Post, J., 1999. Mangenese oxide minerals: crystal structures and economic and environmental significance. Proceedings of the National Academy of Sciences of the United States of America 96, 3447–3454.
Raab, W., 1972. Physical and chemical features of the Pacific deep sea manganese nodules and their implications to the genesis of nodules. In: Horn, D.R. (Ed.), Ferromanaganese Nodules on the Ocean Floor. National Science Foundation, Washington, D.C., pp. 31–50.
Rona, P.A., 1978. Criteria for recognition of hydrothermal mineral deposits in oceanic crust. Economic Geology 73, 135–160.
Roy, S., 1992. Environments and processes of manganese deposition. Economic Geology 87, 1218–1236.
Schaefer, M.O., Gutzmer, J., Beukes, N.J., 2001. Proterozoic Mn-rich oncoids. Earliest evidence for microbially mediated Mn-precipitation. Geology 29, 835–838.
Sevast´yanov, V.F., Volkov, I.I., 1967. Redistribution of chemical elements in the oxidized layers of the Balkan Sea sediments and the formation of manganese nodules. Tr. Inst. Okeanol. 83, 135–152.
Siesser, W.G., Rogers, J., 1976. Authigenic pyrite and gypsum in South West African continental slope sediments. Sedimentology 23, 567–577.
Vodyanitskii, Y.N., Vasilév, A.A., Lesovaya, S.N., Sataev, E.F., Sivtsov, A.V., 2004. Formation of manganese oxides in soil. Eurasian Soil Science 37, 572–584.
Williams, T.M., Bowen, R.B., 1992. Geochemistry and origins of lacustrine ferromanganese nodules from the Malawi Rift, Central Africa. Geochimica et Cosmochimica Acta 56, 2703–2712.
Winter, B., Johnson, C., Clark, D., 1997. Geochemical constraints on the formation of Late Cenozoic ferromanganese nodules from the Central Arctic Ocean. Marine Geology 138, 149–169.